HUNGARIAN UNIVERSITY OF AGRICULTURE AND LIFE SCIENCES

Experimental and DEM model of abrasion of rotary shaft/seal contact with lunar regolith simulants

DOI: 10.54598/007230

PhD. Thesis

by

Hailemariam Shegawu

Gödöllő

2025

Doctoral School and Program denomination:

Doctoral School of Engineering Sciences
Doctoral Program of Mechanical Engineering

Science: Engineering

Head of School: Prof. Dr. László Bozó, MHAS
Institute of Environmental Sciences
Hungarian University of Agriculture and Life Science, Budapest, Hungary

Program leader: Prof. Dr. Gábor Kalácska, DSc
Institute of Technology
Hungarian University of Agriculture and Life Science, Gödöllő, Hungary

Supervisor: Prof. Dr. Gábor Kalácska, DSc
Institute of Technology
Hungarian University of Agriculture and Life Science, Gödöllő, Hungary

Co-Supervisor: Prof. Dr. István Keppler, PhD
Institute of Technology
Hungarian University of Agriculture and Life Science, Gödöllő, Hungary

…… **……**

Affirmation of supervisor(s) Affirmation of head of doctoral program

CONTENT

1. INTRODUCTION, TASKS OF RESEARCH

1.1 Introduction

Abrasive wear remains a persistent challenge in mechanical engineering, particularly for machinery exposed to harsh environments. While terrestrial equipment in mining or agriculture suffers from contaminants like sand, extra-terrestrial environments pose significantly more severe risks to critical components such as bearings, gears, and seals.

Lunar regolith is notorious for its extreme abrasivity. Unlike Earth materials, lunar particles have not undergone atmospheric weathering; consequently, they are highly angular with reactive surfaces that promote aggressive micro-cutting. Even minimal contact accelerates wear, especially in delicate elements like shaft seals where dust infiltration can compromise entire systems.

In contrast, **Martian regolith** is generally coarser and enriched with iron oxides. While Martian dust storms cause wear through persistent deposition, the abrasive potential is somewhat mitigated by the larger, less reactive particle size compared to lunar dust. However, the Moon's harsher characteristics demand a specifically focused evaluation.

Historical lunar missions have confirmed that regolith infiltration leads to the premature degradation of seals, joints, and optical assemblies. Given that on-site repairs in extra-terrestrial settings are impractical, ensuring machinery durability through innovative design and material selection is paramount.

1.2 Tasks of research

This dissertation focuses on the abrasive wear challenges posed by lunar regolith. By analyzing the interaction between abrasive particles and critical machine materials, the research aims to elucidate wear mechanisms and develop robust mitigation strategies to enhance the longevity of future lunar machinery.

Key research tasks include:

- Analysis of lunar dust abrasion on stainless-steel rotary shafts and static seals machined from natural polytetrafluoroethylene (PTFE).
- Coupon-scale laboratory testing using a pin-on-disc machine to measure abrasive friction and wear, supported by microscopic surface analyses.
- Characterization of the regolith simulant, specifically particle shape, profile, and size distribution.
- Development of a Discrete Element Method (DEM) model to simulate the abrasive wear process caused by lunar regolith.
- Sensitivity analysis of the DEM model, examining the influence of parameters such as internal friction, surface energy, and particle geometry.
- Validation of the DEM model using experimental results from the pin-on-disc tests.

2. MATERIALS AND METHODS

2.1 Experimental Materials

Rotary Shaft and Seal Materials

For the rotary shaft counterpart, stainless steel grade 1.4404 (AISI 316L) was selected due to its austenitic structure and low-temperature applicability, which are critical for space environments1. The specific composition includes 17.2% Cr, 10.1% Ni, and 2.1% Mo2. For the static sealing element, a natural Polytetrafluoroethylene (PTFE) was selected as the reference solution. The PTFE samples were machined from "Docaflon" semi-finished rods into 8 x 8 x 8 mm cubes for Pin-on-Disc (PoD) testing.

Abrasive Simulants:

Two lunar regolith simulants were selected to represent different lunar environments:

LHS-1 (Lunar Highland Simulant): A high-fidelity mineral-based simulant composed primarily of Anorthosite (74.4%) and Glass-rich basalt (24.7%). It has a bulk density of 1.30 g/cm^3 and features sub-angular to angular particle shapes5.

LMS-1 (Lunar Mare Simulant): Representing the lunar maria condition, this simulant is composed of Pyroxene (32.8%), Glass-rich basalt (32.0%), and Anorthosite (19.8%). It has a higher bulk density of 1.56 g/cm^3 and sub-rounded to sub-angular particle shapes.

2.2 Experimental Abrasive Pin-on-Disc System

Test Configuration

The abrasion tests were conducted using a Pin-on-Disc (PoD) tribometer (Fig 2.1). The system features a rotating stainless steel disc and a stationary PTFE pin held in a vertical holder. A dust deflector and specific loading mechanisms were employed to simulate the seal-shaft interface under abrasive conditions.

Test Parameters and Procedure

Tests were conducted at room temperature (22–24 °C) with relative humidity between 40–50%RH. The specific operating parameters are detailed in Table 2.1.

Table 2.1. Pin-on Disc test conditions

Parameter	Value / Description
Sliding Speed	0.1 m/s
Normal Load	0.2 MPa
Contact Start	Clean contact
Abrasive Media	LHS-1 or LMS-1 (covering sliding path)
Run Durations	2, 6, 15, and 30 minutes

The working abrasive PoD can be seen on Fig. 2.1.

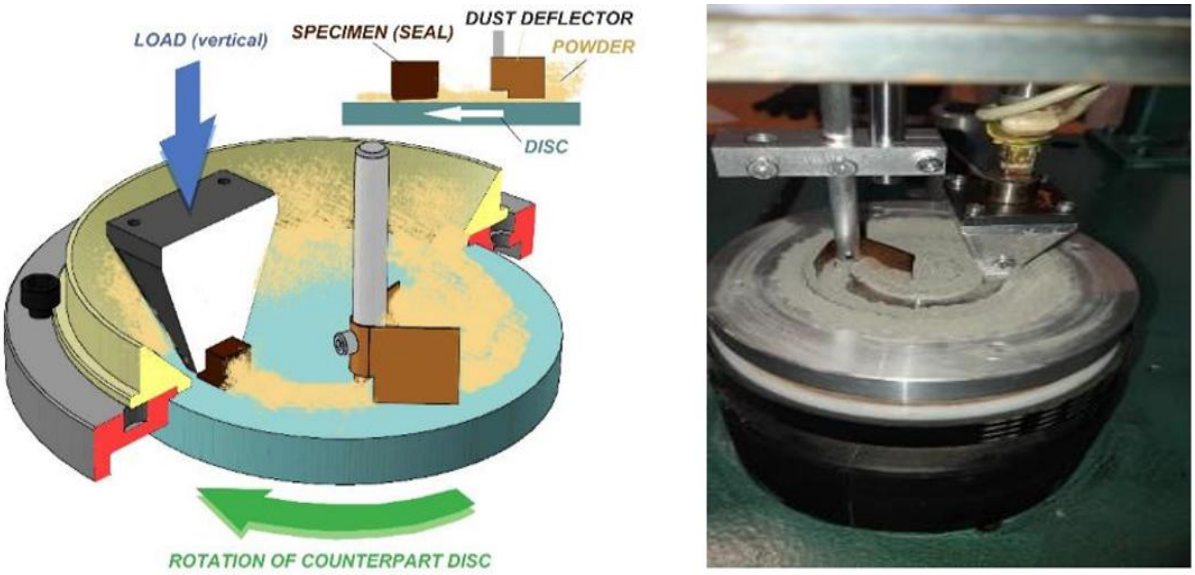

a) Schematic diagram of real machine b) Photo of real machine

Fig.2.1. Pin-on-disc (PoD) abrasive system layout (Kalácska et al., 2024).

Sample Preparation and Measurement Protocol

A strict preparation and characterization protocol was followed for all samples:

- Cleaning: Samples underwent ultrasonic cleaning (Proclean 10.0MS) for 10 minutes using a 1% solution of EM-300 Metallreiniger and osmosis-filtered water, followed by a distilled water rinse.
- Drying: Samples were dried in a DRY30EA cabinet for 24 hours at 22–24°C.
- Pre-Test Characterization: Samples were weighed using an HC5003VG precision balance. Surface roughness (Ra, Rz) was measured using a Mitutoyo SJ-201P tester, and surface morphology was documented via optical microscopy and SEM (Zeiss EVo 40, JEOL JSM-IT700HR).
- Data Processing: Post-test analysis included weight loss calculation, 3D topography analysis (Keyence VR 5200), and EDX elemental analysis of embedded particles.

2.3 Discrete Element Model

Model Framework and Calibration

The research utilized the Discrete Element Method (DEM) to simulate the micro-mechanical interactions between the regolith particles and the machine elements. The simulation parameters were calibrated using the Angle of Repose (AoR) method. Experimental AoR was determined by lifting a hollow cylinder filled with simulant and measuring the resulting pile angle.

- **Experimental AoR (LHS-1):** The average experimental angle was calculated as α_{ave}= 40.09° across five trials.
- **Simulation Setup:** Rocky DEM software was used to replicate these conditions. The simulation utilized polyhedral particle shapes to accurately represent the angularity of lunar dust.

Table 2.2. Material Properties for DEM Input

Property	LHS-1	Stainless Steel (SS)	Natural PTFE
Density (g/cm^3)	1.60	7.95	2.1
Young's Modulus (GPa)	35	200	1.2
Poisson's Ratio	0.25	0.3	0.4

Contact Models and Physics

The interaction between particles and boundary walls was modelled using the Hertz-Mindlin + JKR (Johnson-Kendall-Roberts) model. This selection accounts for the adhesive forces (Van der Waals) relevant to fine powders and micro-scale analysis.

Normal Contact Force (F_c^n)

The total normal contact force is a summation of the Hertzian spring force (Fn,s), damping force (Fn,d), and the JKR adhesive force (Fn,jkr). For a system with "m" contact points, the simplified equation is:

$$F_{tc}^{n} = k_s \sum_{j=1}^{m} a_j^3 - k_d \sum_{j=1}^{m} \delta_{n,j}^{1/4} - k_{jkr} \sum_{j=1}^{m} a_j^{3/2} \quad (2.1)$$

Where:

$k_s = \frac{4E^*}{3R^*}$

$k_d = \frac{2lne\sqrt{m^*E^*}R^{*1/4}}{\sqrt{3ln_e^2+3\pi^2}}\dot{\delta}_n$

$k_{jkr} = \sqrt{8\pi\gamma E^*}$

m Total number of contact points

Tangential Contact Force ($F_{t,s}$): The tangential force includes Hertzian spring and damping components, limited by the Coulomb friction limit. It is described by the Mindlin-Deresiewicz model:

$$F_{Totc}^{t} = -\mu F_{Totc}^{n}\left(1-\zeta^{\frac{3}{2}}\right)\frac{\delta_t}{|\delta_t|} + \eta_t\sqrt{\frac{6\mu m^{*F_{Totc}^{n}}}{\delta_{t,max}}}\zeta^{\frac{1}{4}}\dot{\delta}_t \quad (2.2)$$

Where:

Where μ is the friction coefficient (static or dynamic), δt is the tangential overlap, and ζ represents the ratio of tangential displacement to the maximum limit before sliding occurs.

Motion Integration: Particle motion is resolved using Newton's second law with an explicit time integration scheme. The time step Δt was set to 10% of the critical time step Δt_{crit} derived from the Rayleigh wave speed:

$$\Delta t^{crit} = \frac{\pi r_{min}}{0.163\nu + 0.8766}\sqrt{\frac{\rho}{G}} \tag{2.3}$$

Surface Roughness Generation: To simulate realistic surface interactions, the microstructure of the stainless steel was modelled using Voronoi tessellation. Grain morphology observed via SEM was discretized using Delaunay triangular finite elements. The interaction between a particle and a mesh element is treated as a collision with an immobile particle of identical curvature, using an effective overlap "δ" derived from the particle-element distance $d_{p,e}$.

Wear Model: Abrasive wear was quantified using a modified Archard's equation adapted for DEM. Since sliding distance is not predetermined in dynamic simulations, wear volume (V) is calculated per time step based on resultant velocity (vR):

$$\mathrm{V} = k\frac{\mathrm{F_c^R}\,\mathrm{v_R}\,\Delta t}{H} \tag{2.4}$$

Where:
Where k is the wear coefficient, $\mathrm{F_c^R}$ is the resultant contact force, H is hardness, and vR as follows:

$\mathrm{v_R}$ Resultant velocity, $\mathrm{v_R} = \sqrt{\dot{\delta}_t^2 + \dot{\delta}_n^2} = \sqrt{\mathrm{v_t^2} + \mathrm{v_n^2}}$

3. RESULTS AND DISCUSSION

3.1 Pin-on-disc abrasive measurements with LHS1 regolith

Friction and wear behaviour

The tribological behaviour of the Stainless Steel (SS) and PTFE pair against LHS1 lunar regolith simulant was characterized by the coefficient of friction and vertical displacement.

Friction Evolution: The tests began with a distinct run-in phase (first 8-10 meters), where pure PTFE/steel adhesive contact resulted in a peak friction coefficient of approximately 0.35. Following this, LHS1 particles entered (Fig.3.1) the contact zone, transitioning the system to a stable sliding resistance (~0.2) governed by a Berthier-Eleőd three-body abrasion mechanism. Recurring friction peaks every 10 meters indicated particle agglomeration and congestion within the contact zone.

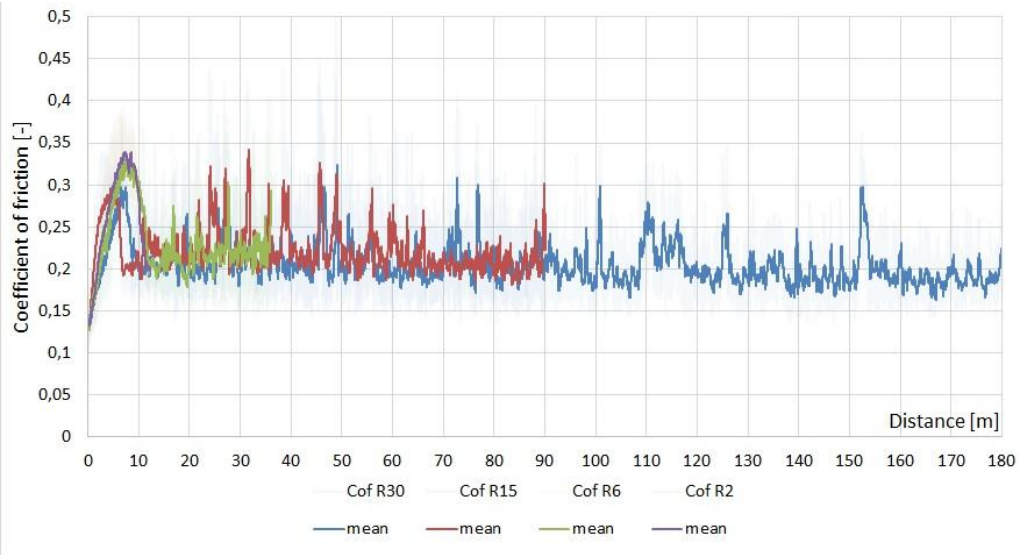

Fig.3.1. Summary of friction results (Ln-SS-LHS1-R2-R6-R15-R30).

Vertical Displacement of pin holder head (Wear): The vertical displacement curves revealed a "negative wear" phenomenon. (example for LHS1, Fig 3.2) After the initial adhesive phase, the ingress of regolith physically lifted the pin holder, causing negative displacement readings between 10 and 50 meters. Extreme peaks (down to -0.5 mm) indicated large particle agglomerates. After 50-60 meters, the system stabilized into a linear abrasive wear trend due to continuous micro-cutting, reaching a total displacement of 0.1 mm.

Surface characterization

Disc Surface: SEM analysis of the stainless steel disc (Fig 3.3) confirmed a dominant micro-ploughing mechanism. Wear progressed from initial scratching (R2) to distinct parallel bands of damage (R15, R30). The Degree of Penetration (Dp) values were consistently below 0.1 (0.052 at R2 to 0.043 at R30), indicating that material was plastically deformed into ridges rather than removed. Elemental analysis (EDX) confirmed the accumulation of mineral phases (Al, Si, Ca) and Fluorine transferred from the PTFE pin.

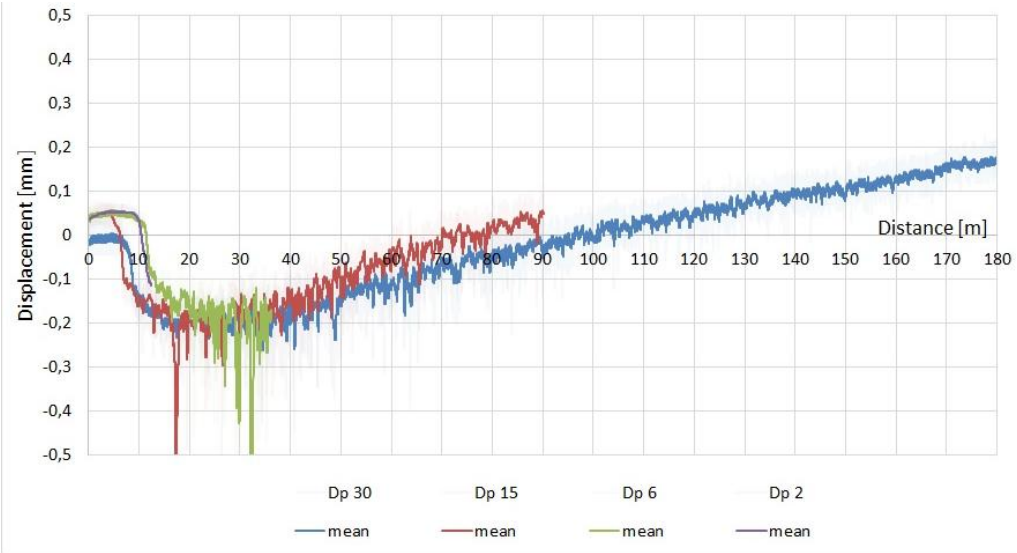

Fig.3.2. "Wear" curves showing the vertical displacement of the pin holder.

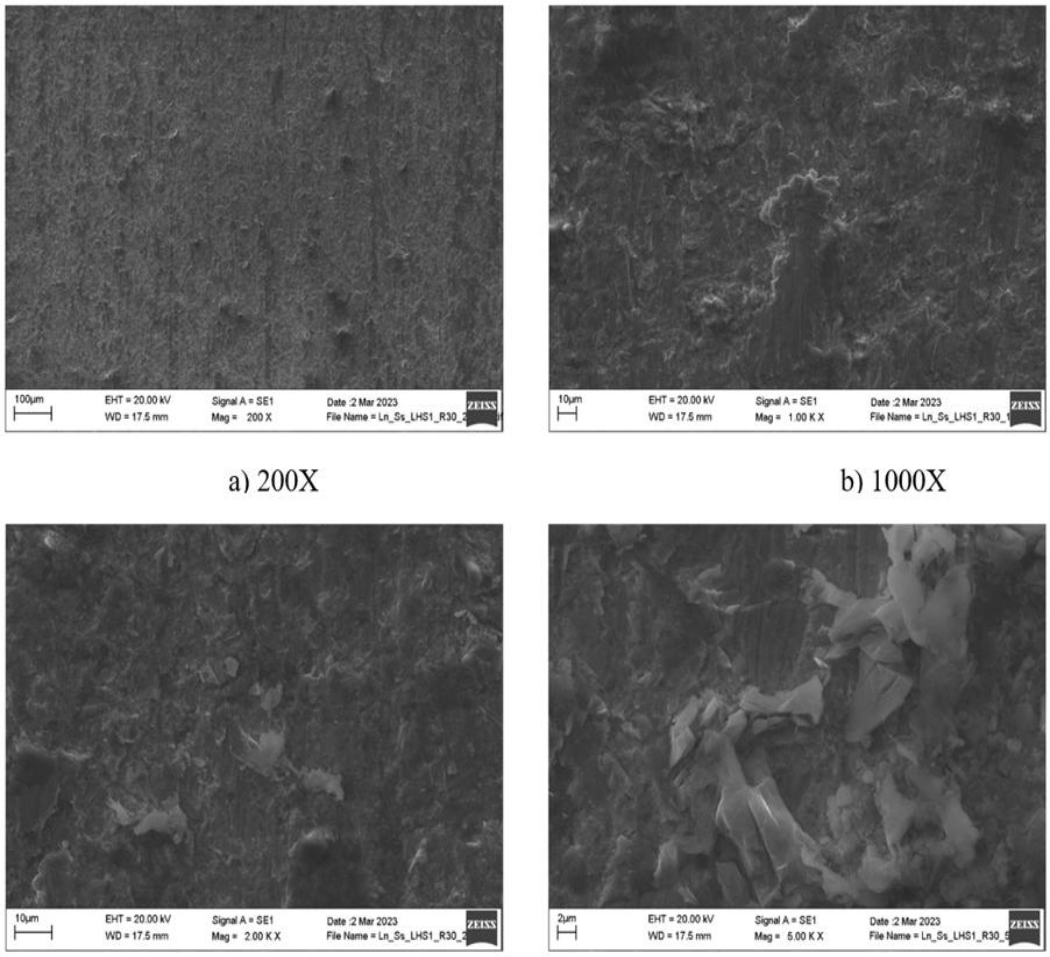

Fig.3.3. SEM image of the R30 worn disc surface at high different magnification, showing increased damage density and embedded particles.

Pin Surface: The PTFE pin exhibited a mixed-mode wear mechanism. Large particles (>40 µm) embedded quickly, while harder particles acted as cutting tools. (Fig. 3.4) The wear evolved from particle embedding (R2) to deep abrasive groove bands (R30). The Dp values for the pin were significantly higher (0.197–0.244), confirming significant material removal via micro-cutting.

pieces, though the latter is considered less likely given that the PTFE is much softer than the LHS1 particles.

a) Ln-SS- LHS1-R2 Pin b) Ln-SS- LHS1-R30 Pin

Fig.3.4. Microscopic image (50x) of abrasive grooves and embedded particles of LHS1.

3D Surface topography analysis

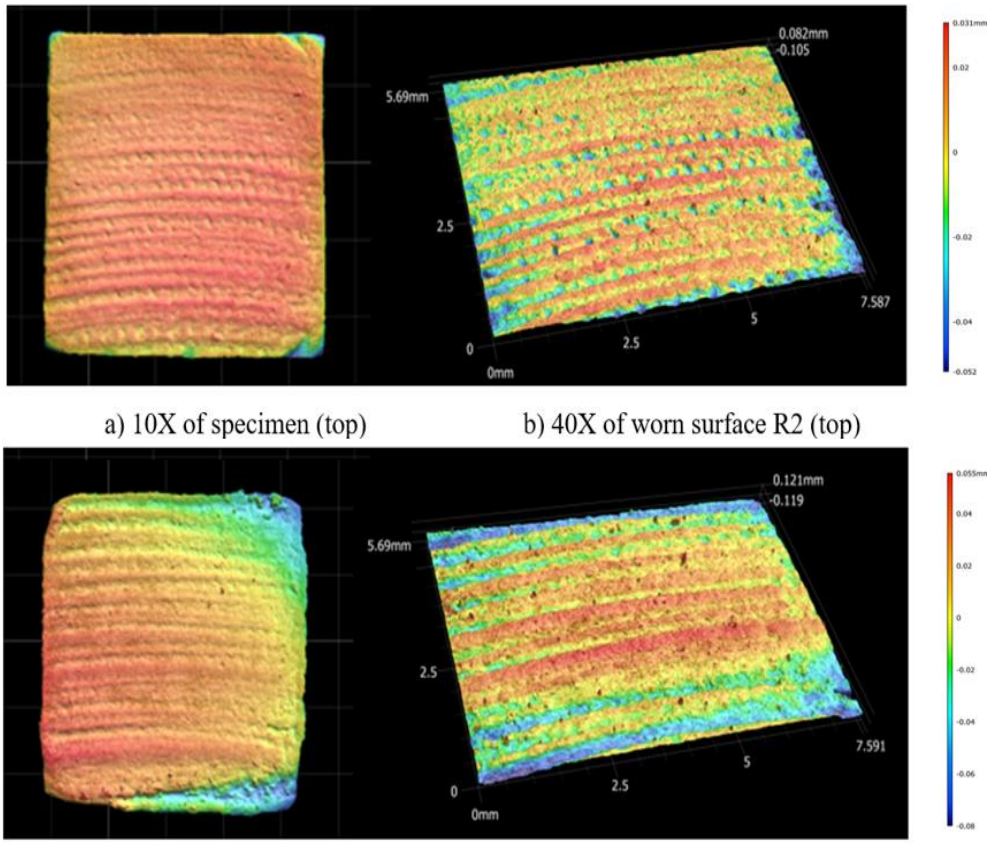

a) 10X of specimen (top) b) 40X of worn surface R2 (top)

c) 10X of specimen (bottom) d) 40X of worn surface R30 (bottom)

Fig.3.5. 3D image of specimen and worn surfaces of the PTFE pin.

3D topography confirmed the presence of "particle-filled ridges" along the wear tracks. (Fig. 3.5) The slightly higher Dp on smaller radii (R2/R15) suggested greater stress-torsion due to track curvature. On the pin, the surface initially smoothened but roughened again by R30 due to embedded particles.

3.2 Pin-on-disc abrasive measurements with LMS1 regolith

Friction and wear analysis

Experiments with LMS1 (Lunar Mare Simulant) demonstrated a similar three-body mechanism but with higher severity.

- Friction: The initial adhesive run-in reached a higher peak of ~0.4 compared to LHS1. The stabilized friction fluctuated between 0.2 and 0.3, indicating a less stable interaction. (Fig 3.6)
- Wear: The "pin lift" effect was more pronounced, with negative displacement peaks reaching -0.7 mm due to larger particle blockages (Fig. 3.7). The total vertical displacement reached 0.1 mm, showing higher abrasivity than LHS1. (More steep linear wear trend).

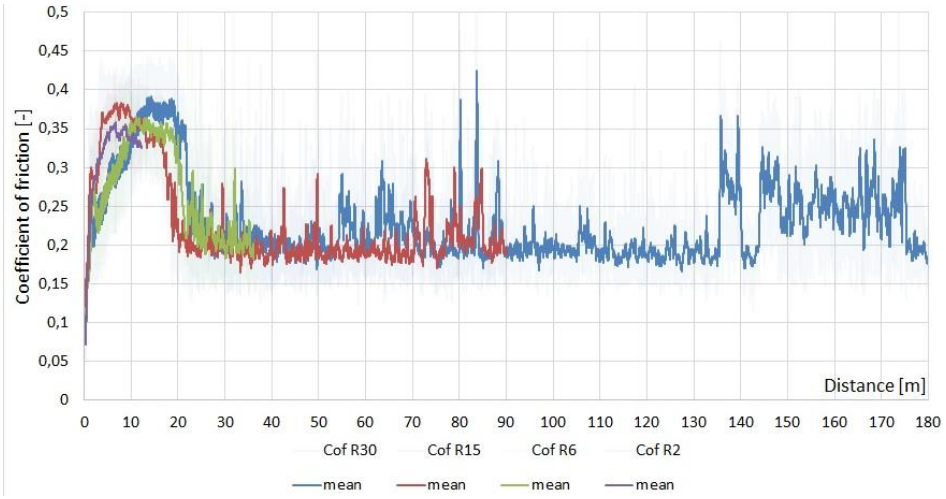

Fig.3.6. Summary of friction results (Ln-SS-LMS1-R2-R6-R15-R30).

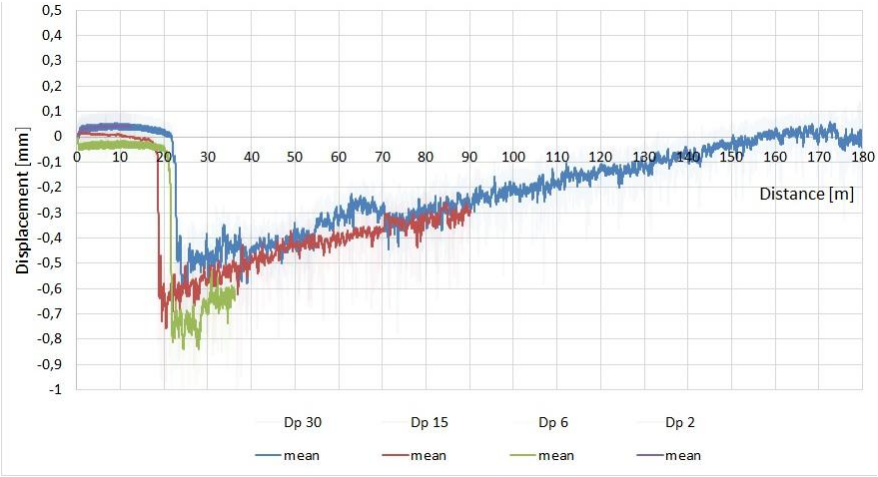

Fig.3.7. "Wear" curves showing the vertical displacement of the pin holder.

Surface characterization

Disc: The disc showed increasing damage density and embedded particles (calcium silicates, olivine, ilmenite). EDX analysis showed a significant increase in Si (7.68 wt%) and Al (4.81 wt%) by R30.

Pin: The PTFE surface became completely covered in abrasive dust. By R30, deep cut abrasive groove bands formed between densely embedded particles, creating a consistent abrasive layer.

3D Surface topography

The Dp values for the disc decreased with time (0.044 at R2 to 0.024 at R30), suggesting a "softening" effect as regolith particles filled the wear grooves. Conversely, the pin Dp values peaked at R6 (0.372) before stabilizing, indicating aggressive micro-cutting early in the process (Fig 3.8).

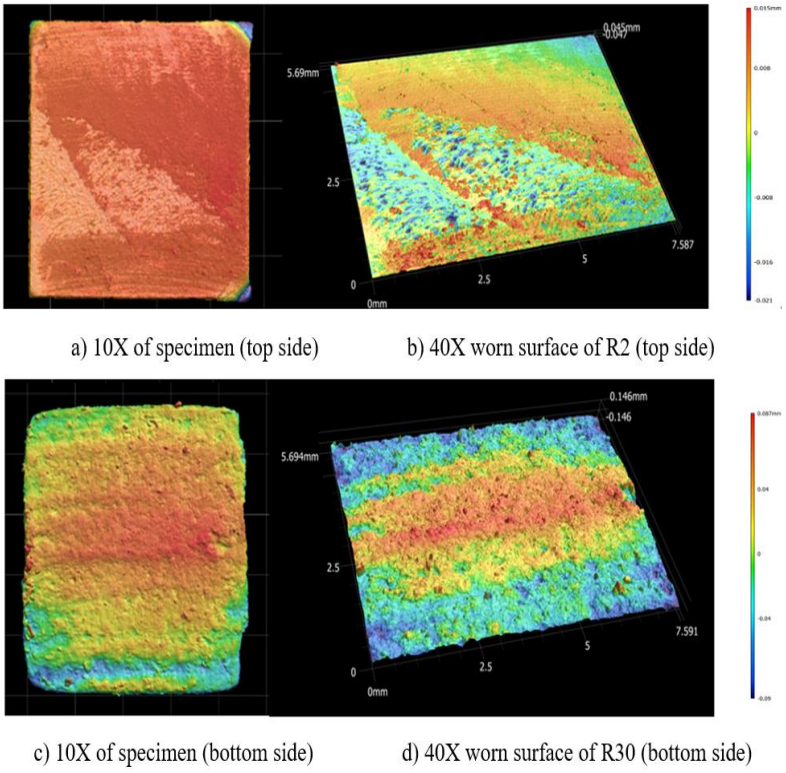

Fig.3.8. 3D image of worn pin surface by LMS1.

Comparative analysis (LHS1 vs. LMS1)

While both simulants induced a three-body abrasive mechanism, LMS1 proved consistently more severe. LMS1 caused 50% more total wear and a 40% greater pin lift during the ingress phase. Although LHS1 particles embedded more readily into the steel disc (higher Si/Al concentrations in EDX), LMS1 formed a thicker, more unstable third-body layer in the contact zone (Table 3.1)

Table 3.1. Summary of tribological features

Parameter	**LHS1 (Highland)**	**LMS1 (Mare)**	**Key difference**
Peak CoF (Run-in)	~0.35	~0.4	LMS1 is ~14% higher
Stabilized CoF	~0.2 (stable)	0.2- 0.3 (variable)	LMS1 is higher and less stable
Max. negative wear	-0.5 mm	-0.7 mm	LMS1 causes 40% greater pin lift
Total Displacement	up to 0.1 mm	up to 0.15 mm	LMS1 causes 50% more wear
Disc wear micro-Mechanism	Micro-ploughing	Micro-ploughing	Similar mechanism
Pin wear micro-mechanism	Mixed	Mixed (High cutting)	LMS1 shows more significant micro-cutting

3.3 Numerical simulations (DEM)

Discrete Element Method (DEM) simulations were employed to extend predictive capabilities beyond specific experimental configurations. The workflow (Fig. 3.9) involved calibrating bulk behaviour (angle of repose) and tribological wear coefficients.

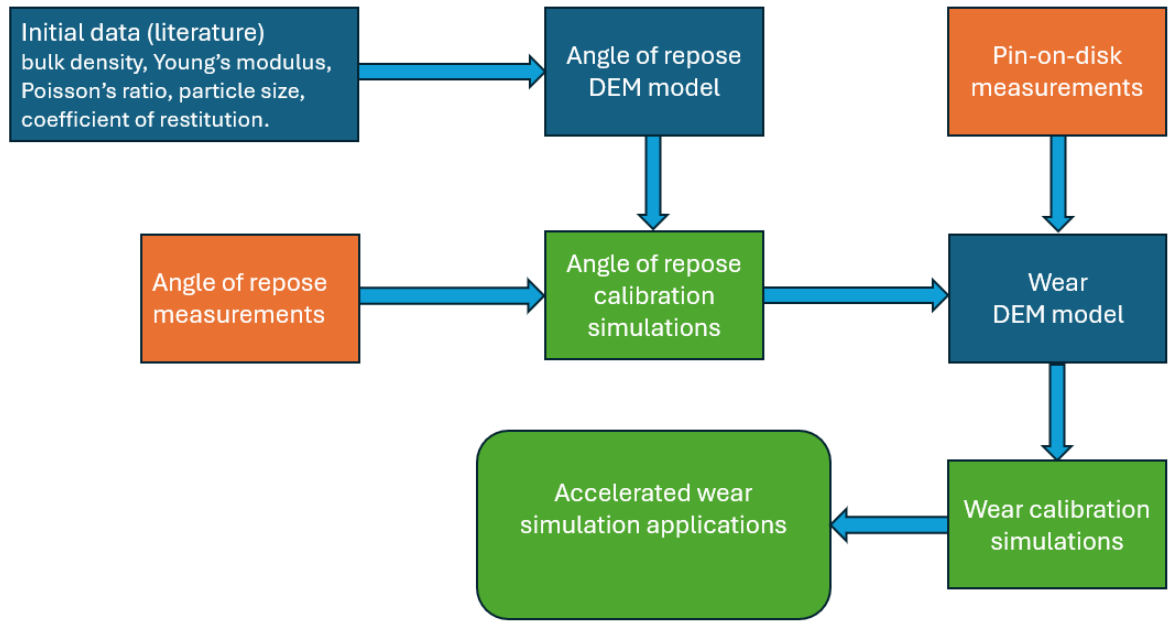

Fig.3.9. Workflow of data sources, calibration, and DEM-based wear modelling.

Angle of repose measurements

The angle of repose served as a proxy for bulk stability and interparticle friction. LHS1 (angular) formed significantly steeper heaps (34°±1.4) compared to the smoother LMS1 (29°±1.2) (Fig. 3.10).

a) LHS-1 b) LMS-1

Fig.3.10. Angle of repose test example photos

Angle of repose numerical model

A cylindrical lift test was simulated using polyhedral particles to calibrate the DEM parameters (Fig. 3.11).

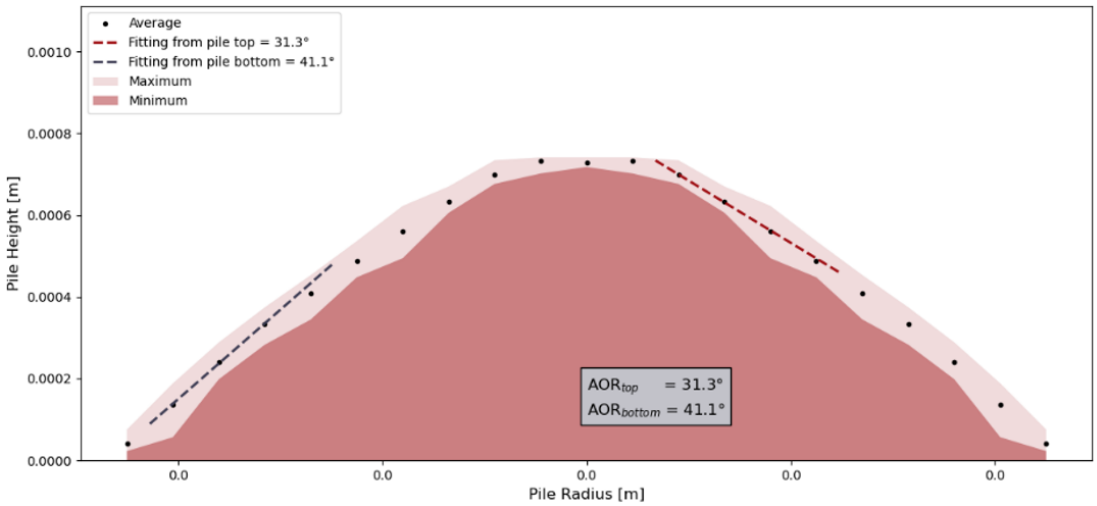

Fig.3.11. Angle of repose test result example

To create a predictive framework, functional relationships between micromechanical parameters and the angle of repose (φ) were derived:

1. Friction Dependence: The relationship between the angle of repose and static friction (μ_0) followed a logistic function (R^2=0.981):

$$\varphi(\mu_0) = \frac{L}{1+e^{-k(\mu_0-\mu_i)}} + \varphi_0 \quad (3.1)$$

This expression captures the essential mechanical behaviour of granular materials,

Where:

$\varphi(\mu_0)$ Angle of repose

μ_0 Interparticle static friction coefficient

$L = 41{,}22°$ Maximal increase in angle attributable to frictional effects

$k = 6.11$ Characterizes the sensitivity of the angle to changes in friction

$\mu_i = 0.12$ Inflection point indicating the most responsive friction range

$\varphi_0 = 1.88°$ Base angle of repose in the hypothetical limit of zero friction

$$\varphi(\mu_0) = \frac{L}{1+e^{-k(\mu_0-\mu_i)}} + \varphi_0 \quad (4.1)$$

This expression captures the essential mechanical behaviour of granular materials (Fig 3.12),

Where:

$\varphi(\mu_0)$ Angle of repose

μ_0 Interparticle static friction coefficient

$L = 41{,}22°$ Maximal increase in angle attributable to frictional effects

$k = 6.11$ Characterizes the sensitivity of the angle to changes in friction

$\mu_i = 0.12$ Inflection point indicating the most responsive friction range

$\varphi_0 = 1.88°$ Base angle of repose in the hypothetical limit of zero friction

This captures the saturating nature of friction, where the system stabilizes near a structural limit.

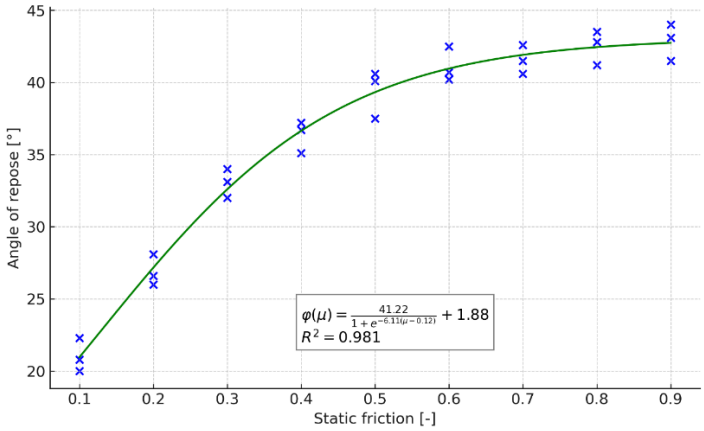

Fig.3.12. Angle of repose as a function of the interparticle static friction coefficient.

2. Adhesion Dependence**:** Adhesive surface energy (E) was found to have a linear relationship with the angle of repose (R^2=0.9821), serving as an effective surrogate for geometric interlocking:

$$\varphi = 272.61 \cdot E + 30.32 \quad (R^2 = 0.9821) \quad (3.2)$$

Where:

φ Angle of repose
E Adhesive surface energy
$R^2 = 0.9821$ High coefficient of determination

Wear simulations

A "pin slice" model was developed to reproduce the pin-on-disc wear without prohibitive computational costs. A representative slice of the pin interacted with regolith particles under 0.2 MPa pressure (Fig.3.13).

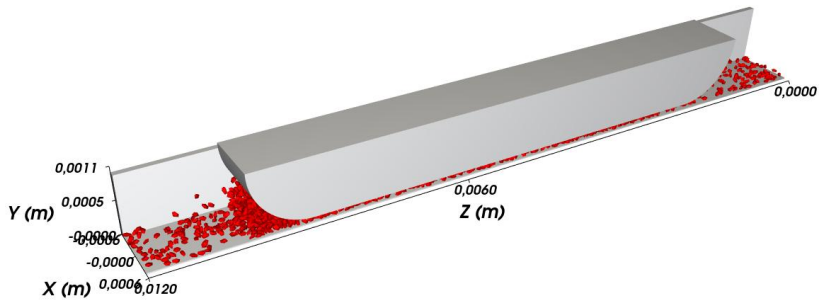

Fig.3.13. Simplified DEM model of the pin slice in contact with LHS-1 regolith particles.

Calibration: The wear coefficient (k) was systematically varied to match the experimental volume loss. A robust linear scaling law was established across four orders of magnitude (R^2=0.9998):

$$d = 1.4814k \tag{3.3}$$

Where „d" is the worn-out material thickness. (Fig.3.14.) This linearity enables accelerated wear modelling: simulations can be run with artificially high wear coefficients and the results reliably rescaled, bypassing the need for computationally expensive simulations with real-time wear rates.

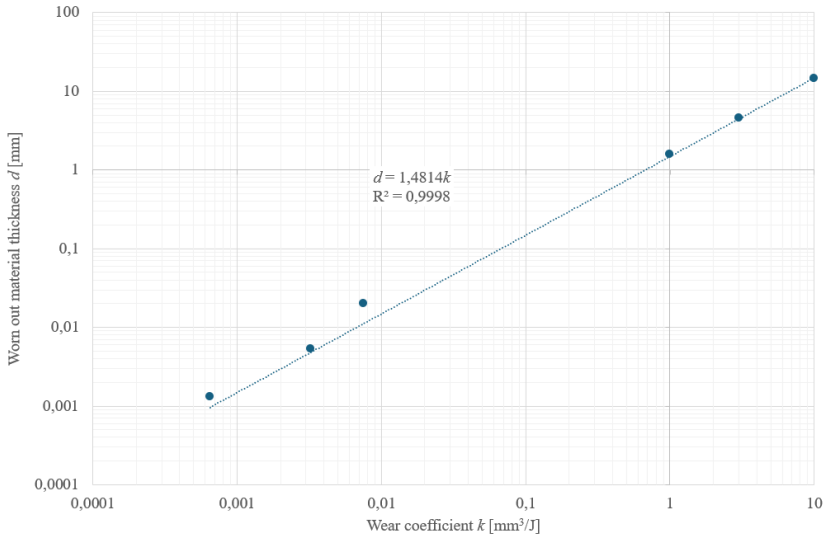

Fig.3.14. Correlation between the wear coefficient *k* and the worn-out material thickness "*d*"

4. NEW SCIENTIFIC RESULTS

1. With my experimental measurements, I confirmed that both the LHS1 and LMS1 lunar regolith simulants induce a third-body abrasive wear mechanism for the stainless steel and PTFE pairing. This process is characterized by particle embedment and dynamic friction processes (steady state) after the running-in phase. Through on-line measurements and detailed post-test analyses (SEM, EDX, 3D surface topography), the study confirmed that both simulants induce third-body abrasive wear, but their distinct compositions result in significant differences in friction and wear kinetics and a linear wear trend developed, consistent with the Rabinowicz and Hutchings wear-model. The LMS1 particles, entering the contact zone after a longer sliding path, formed a 200-250% thicker regolith layer between the PTFE and stainless steel (SS) surfaces. The resulting steady-state wear phase is also linear, but steeper compared to the LHS1.

2. Based on my experiments, analysing the Dp (Degree of Penetration) values, I highlighted that the LHS1 and LMS1 regoliths induce different abrasive micro-mechanisms. On the stainless steel (Ss) disc, I observed low Dp values for both regoliths (LHS1: 0.043-0.052; LMS1: 0.024-0.044), which indicates the dominance of micro-ploughing. This suggests that the particles partially embed into the steel's micro-geometry, plastically deforming the steel and reducing the surface roughness. In contrast, on the PTFE pin, the Dp values are higher and show a significant difference. For the LHS1, the Dp values (0.197-0.244) indicate a mixed wear mechanism where micro-ploughing and micro-cutting are in balance. However, the LMS1 regolith, due to its higher ilmenite and pyroxene content, causes more aggressive micro-cutting—in line with the wear curve—which is supported by the exceptionally high Dp value (R6: 0.372). This phenomenon can be traced back to the more intensive material removal caused by the harder LMS1 particles. Through the Dp metric, I proved that the different mineral compositions of the regoliths fundamentally influence the nature of the abrasive mechanisms on both hard and softer surfaces.

3. From DEM modelling, I established functional relationship between interparticle friction and the angle of repose. The relationship between the angle of repose (φ) and the interparticle static friction coefficient (μ_0) was found to follow a logistic-type saturation law of the general form

$$\varphi(\mu_0) = \frac{L}{1 + e^{-k(\mu_0 - \mu_i)}} + \varphi_0 \,.$$

For the simulated polyhedral lunar regolith assembly, the fitted parameters were: $L = 41{,}22°$ maximal increase in angle attributable to frictional effects, $k = 6.11$ the sensitivity of the angle to changes in friction, $\mu_i = 0.12$ inflection point indicating the most responsive friction range, $\varphi_0 = 1.88°$ base angle of repose in the hypothetical limit of zero friction. The model accurately describes the data over the range $0 \leq \mu \leq 0.8$ with a coefficient of determination $R^2 = 0.981$. This functional form captures the transition from highly mobile, low-friction particle systems to geometrically constrained, high-friction packings and provides a physically interpretable constitutive law for regolith heap stability.

4. Using DEM I set the dependence of the angle of repose on adhesive surface energy. At a constant friction level, the angle of repose (φ) increases linearly with the adhesive surface energy (E), expressed generally as

$$\varphi = a \cdot E + b$$

Where: $a = 272.61\ \frac{\text{degree}}{\text{mJ}}$, $b = 30.32°$, yielding an excellent correlation with $R^2 = 0.9821$ over the range $0.01 \leq E \leq 0.1\ \frac{\text{mJ}}{\text{m}^2}$. This result demonstrates that adhesion effectively reproduces the enhanced bulk stability typical of cohesive and angular regoliths, providing a practical surrogate parameterization for electrostatic and vacuum-sintered interparticle bonding effects in DEM simulations.

5. I concluded the relation between wear coefficient and worn material thickness for LHS-1 simulant. The DEM-based wear calibration performed with the LHS-1 lunar highland simulant revealed a linear scaling law between the wear coefficient (k) and the resulting worn-out material thickness (d) of the general form

$$d = c\,k.$$

The regression analysis yielded $c = 1.4814\ \text{Jmm}^{-2}$ with a coefficient of determination $R^2 = 0.9998$, valid within the range $10^{-13} \leq k \leq 10^{-9}\text{m}^3\text{J}^{-1}$. This linearity confirms the direct proportionality between the wear coefficient and the total material loss, enabling the use of accelerated wear simulations where artificially increased k values can be employed and rescaled through the established relation. The result provides a transferable quantitative tool for predicting regolith-induced wear on polymeric materials under lunar surface conditions.

5. CONCLUSIONS AND PROPOSALS

My study provided a comprehensive tribological evaluation of stainless steel (1.4404) and natural PTFE contact pairs exposed to two lunar regolith simulants (LHS1 and LMS1), supported by extensive microscopy, 3D topography, elemental analysis, and DEM-based numerical modelling. The experimental results revealed that both simulants produce a characteristic three-body abrasive mechanism, initiated after an adhesive PTFE–steel run-in phase and sustained by the dynamic ingress, embedment, and rolling of mineral particles within the contact zone.

For both simulants, the stainless-steel counterface exhibited a dominant micro-ploughing mechanism, confirmed by low Dp values (<0.1), progressive groove formation, and increasing particle embedment. In contrast, the PTFE pins experienced a mixed wear mechanism of micro-ploughing and micro-cutting, where embedded grains acted as cutting tools and produced deep, directional abrasive grooves with increasing sliding distance. LMS1 consistently produced greater friction, higher wear rate, and more severe micro-cutting than LHS1, indicating its higher abrasivity and dynamic instability.

Numerical simulations successfully reproduced bulk particle behaviour and provided a calibrated DEM model capable of predicting changes in angle of repose as a function of interparticle friction and cohesion. Furthermore, the DEM wear framework demonstrated its applicability for reproducing micro-scale abrasive interactions, establishing a transferable modelling workflow adaptable to other extra-terrestrial soils such as Martian dust. This dual experimental-numerical approach forms a robust foundation for predicting component longevity and designing abrasion-resistant mechanisms for planetary surface operations.

Proposals

- Improve sealing materials for lunar environments:

Based on severe micro-cutting observed on PTFE, alternative materials such as filled PTFE composites, polyimides, or reinforced elastomers should be tested to reduce material removal and extend component life.

- Applications of engineered surface treatments on steel counterfaces:

Hard coatings (DLC, nitriding, ceramic PVD layers) or texturing strategies may reduce particle embedment and micro-ploughing. Surface engineering should be explored using the DEM wear model prior to prototyping.

- Optimize seal/shaft geometries through DEM-based pre-screening:

Since DEM wear simulations reproduce regolith interactions at the particle level, they should be used to evaluate contact pressure, track curvature, and groove geometry before manufacturing large-scale test hardware.

- Extend abrasion studies to vacuum and thermal-cycling conditions:

Lunar surface mechanisms operate under extreme temperatures and near-vacuum, which affect PTFE deformation, regolith adhesivity, and third-body dynamics. Replicating these conditions will improve prediction accuracy.

- Investigate multi-particle size distributions and long-duration wear

Real regolith contains extreme fines (<20 μm) and sharp agglutinates, which likely intensify wear beyond the simulants tested. Incorporating fines into experiments and simulations will create more realistic abrasive conditions.

6. SUMMARY

This dissertation, "Experimental and DEM model of abrasion of rotary shaft/seal contact with lunar regolith simulants," addresses the critical challenge of abrasive wear in machinery designed for extra-terrestrial environments, focusing specifically on the highly destructive nature of lunar regolith. The core objective was to develop and validate a robust modelling framework by integrating empirical data from coupon-scale tribological tests with advanced Discrete Element Method (DEM) numerical simulations.

The experimental phase utilized a Pin-on-Disc (PoD) setup to simulate the sliding contact between a stainless steel (SS) disc and a Polytetrafluoroethylene (PTFE) pin, representing a typical shaft/seal interface. The abrasive media consisted of two distinct mineralogical simulants: LHS1 (Anorthosite-rich, Lunar Highland Simulant) and LMS1 (harder, Ilmenite/Pyroxene-rich, Lunar Mare Simulant). Through on-line measurements and detailed post-test analyses (SEM, EDX, 3D surface topography), the study confirmed that both simulants induce third-body abrasive wear, but their distinct compositions result in significant differences in friction and wear kinetics. The softer LHS1 led to a milder tribological response, while the harder LMS1 formed a 200–250% thicker regolith layer and caused higher local friction instabilities. A key finding was the distinction in abrasive micro-mechanisms: the wear on the hard SS disc was dominated by micro-ploughing for both simulants, whereas on the soft PTFE pin, LHS1 induced a mixed wear mechanism (ploughing and cutting), and the aggressive LMS1 caused significantly more detrimental micro-cutting, quantifiable by the exceptionally high Degree of Penetration metric (Dp up to 0.372).

New scientific results emerged from the development of the numerical model. The DEM framework was calibrated by establishing a non-linear logistic relationship (R^2=0.981) between the Angle of Repose (AoR) and the interparticle friction coefficient, allowing for a transferable calibration framework applicable to various regolith simulant batches. Crucially, the DEM simulation established a direct proportionality between volumetric material loss and shear work input for the PTFE specimen. This novel relationship allows for accelerated wear modelling, where researchers can artificially increase the wear coefficient in the simulation and rescale the results, effectively bypassing the enormous computational expense associated with using the actual, high Young's modulus of regolith particles. In conclusion, the research successfully quantified the differential abrasive behaviour of two key lunar regolith types and delivered a validated, computationally efficient DEM-based predictive tool for designing more resilient shaft/seal systems for future deep-space exploration missions.

7. ACKNOWLEDGEMENT

This research is closely connected to the ESA research project 4000136800/21/NL/CBi, in which I actively participated. I would like to express my sincere gratitude to the members of the research group at the Institute of Technology, MATE, for their valuable support and collaboration. Special thanks are extended to Dr. Ádám Kalácska (University of Ghent) for his assistance with 3D surface topography, and to Dr. Zoltán Károly (HUN-REN) for his help with SEM and EDX analyses.

8. DECLARATION ON THE USE OF ARTIFICIAL INTELLIGENCE

I hereby declare that the research and intellectual content of this dissertation are my own original work, under the guidance of my supervisors and sometimes in collaboration with a research team, except where explicitly noted. The core intellectual contributions, including the research questions, data collection, analysis, and interpretation, are entirely my responsibility.

Specific Use of Artificial Intelligence (AI) Software

AI software: Gemini 2.5 Flash, Chat GPT was used exclusively to refine language and expression: Act as an advanced language polishing and editing aid to enhance the clarity, fluency, and professional English expression of the final written text. This included correcting grammar, improving sentence structure, and suggesting precise terminology.

Exclusion of AI in Content Generation

I confirm that AI software **was not used** for:

- Generating any original research ideas, hypotheses, or theoretical frameworks.
- Creating or modifying the core content, including the literature review, methodology, results, or discussion sections.
- Any form of data collection, manipulation, or interpretation.
- The creation or modification of figures, tables, or graphical elements.

The substance and intellectual originality of this dissertation remain my sole responsibility, supported by my supervisors' guidance.

Signature:

Date: 18/11/2025

9. MOST IMPORTANT PUBLICATIONS RELATED TO THE THESIS

1. Hailemariam Shegawu, István Oldal, Gábor Kalácska: Abrasive wear by experimental methods with three-body abrasive wear testers. Mechanical Engineering Letters, 2021, vol. 21. pp 61 -77. HU ISSN 2060-3789
2. Shegawu Hailemariam, István Oldal, Gábor Kalácska: A Review of Abrasive Wear by Coupled Finite and Discrete Element Methods, SCIENTIFIC BULLETIN, Serie C, Fascicle: Mechanics, Tribology, Machine Manufacturing Technology, ISSN 1224-3264, Vol. 2021 No.XXXV
3. Hailemariam Shegawu, István Oldal, Gábor Kalácska: A review of three body abrasive wear by combined finite element method with smooth particle hydrodynamics and discrete element method. Mechanical Engineering Letters, 2021, vol. 21. pp 96 -110. HU ISSN 2060-3789
4. István Oldal, Hailemariam Shegawu, Gábor Kalácska: Finite element method of frictional sliding contact between pin and disc tribology model. Mechanical Engineering Letters, 2021, vol. 24. pp 126 -148. HU ISSN 2060-3789
5. György Barkó, Gábor Kalácska, Róbert Keresztes, László Zsidai, Hailemariam Shegawu, Ádám Kalácska: Abrasion Evaluation of Moon and Mars Simulants on Rotating Shaft/Sealing Materials: Simulants and Structural Materials Review and Selection: Lubricants 2023, 11(8), 334; DOI: 10.3390/lubricants11080334
6. Gábor Kalácska, György Barkó, Hailemariam Shegawu, Ádám Kalácska, László Zsidai, Róbert Keresztes and Zoltán Károly: The Abrasive Effect of Moon and Mars Regolith Simulants on Stainless Steel Rotating Shaft and Polytetrafluoroethylene Sealing Material Pairs. Materials 2024, 17, 4240. DOI: 10.3390/ma17174240